Hydrate-phobic Surfaces: Fundamental studies in clathrate hydrate adhesion reduction

By *J. David Smith*, *Adam J. Meuler*, *Harrison Bralower*, *Rama Venkatesan*, *Siva Subramanian*[3], *Robert E. Cohen*, *Gareth H. McKinley*, and *Kripa K. Varanasi**

Clathrate hydrate formation and subsequent plugging of deep-sea oil and gas pipelines represent a significant bottleneck for deep-sea oil and gas operations and expansion to greater depths. Current methods for hydrate mitigation are energy intensive and environmentally unfriendly, comprising chemical, thermal, or flow management techniques. In this paper, we present an alternate approach of using functionalized coatings to reduce hydrate adhesion to surfaces, ideally to a low enough level that hydrodynamic shear stresses can detach deposits and prevent plug formation. Systematic and quantitative studies of hydrate adhesion on smooth substrates with varying solid surface energies reveal a linear trend between hydrate adhesion strength and the practical work of adhesion ($1+\cos\theta_{rec}$) of a suitable probe liquid, that is, one with similar surface energy properties to those of the hydrate. A reduction in hydrate adhesion strength by more than a factor of four when compared to bare steel is achieved on surfaces characterized by low Lewis acid, Lewis base, and van der Waals contributions to surface free energy such that the practical work of adhesion is minimized. These fundamental studies provide a framework for the development of hydrate-phobic surfaces, and could lead to passive enhancement of flow assurance and prevention of blockages in deep-sea oil and gas operations.

1. Introduction

The most recent world energy outlook predicts that energy demand in 2035 will be 36% higher than in 2008.[1] The Department of Energy and the oil and gas industry are looking at ultra deep-sea exploration as a next frontier for meeting these increasing global energy needs. However, many challenges need to be overcome before drilling and production at greater depths becomes economical. One pressing challenge is the formation of natural gas hydrates

in oil and gas pipelines.[2] Hydrates are crystalline structures consisting of a lattice of water cages that entrap hydrocarbon molecules at elevated pressures and low temperatures.[2] Hydrates can plug oil lines, forcing operations to stop until they are removed, and in some extreme events, can pose safety issues by forming a projectile within the line if subjected to large differential pressures.[3] Recently, hydrates were a key reason for the failure of the containment box approach to oil recovery after the recent Gulf spill. Hydrates clogged the opening of the box near the sea floor, preventing oil from being siphoned to boats on the surface.[4] Current methods for hydrate mitigation focus on the use of chemicals to shift the equilibrium hydrate formation curve to higher pressures and lower temperatures, using kinetic inhibitors to slow the growth of hydrates, and insulating or heating the pipeline walls.[5-7] The costs associated with these methods and with lost oil and gas production due to hydrate plugging can run into billions of dollars (more than $200 M USD is spent annually on hydrate inhibiting chemicals alone[3]). Furthermore, these methods are energy intensive and environmentally unfriendly, and alternative approaches to reduce hydrate adhesion are of great interest.

In this paper, we study a new approach for preventing hydrate plug formation: reducing hydrate adhesion strength to surfaces using functionalized coatings. We develop a fundamental understanding of hydrate adhesion as a function of surface energy properties and provide tools for straightforward design of low hydrate adhesion surfaces, i.e., "hydrate-phobic surfaces". The approaches laid out in this paper could provide a pathway to develop hydrate-phobic coatings for enhanced flow assurance and enable oil and gas production from ultra-deep sea reserves.

While hydrate nucleation and formation have been described in the literature[7-16], there are relatively few studies on hydrate adhesion. Most adhesion studies to date have used a micromechanical adhesion testing apparatus to measure adhesion forces between hydrate particles, or between hydrate and ice particles.[17-20] A few investigations have examined the

effect of surface wettability on capillary forces between hydrate particles and surfaces.[21, 22] These studies concluded that the deposition of hydrate particles from the fluid bulk onto the pipeline wall is unlikely, because the capillary forces involved are insufficient to maintain adherence of the hydrate particles under flow conditions. However, much higher adhesion forces were reported for hydrates that were grown directly on a surface[21], indicating that hydrates that form on pipeline walls would likely remain adhered under hydrodynamic forces and providing evidence that their adhesion is governed by forces other than capillary forces. The effect of wettability and surface energy on the adhesion strength of gas hydrates that form directly on a surface has not been explored. In this paper we systematically investigate the effect of wettability and surface energy on hydrate adhesion strength.

This work was inspired by numerous studies of the relationships between water wettability and ice adhesion strength that were summarized in detail in our previous work on ice adhesion[23] and are briefly described here. Petrenko and Whitworth compiled ice adhesion strength and water contact angle data from several research groups on a single plot and found that while ice adhesion strength generally decreased with increasing water contact angle, significant scatter was present in the data.[24] We expanded upon this work by investigating relationships between ice adhesion strength and various measures of water wettability on surfaces with varying chemistry, [23] and reported a strong linear correlation between the practical work of adhesion for liquid water, which is calculated from receding contact angles (i.e. $W^{a}_{water,rec} = \gamma_{water}(1+\cos\theta_{rec})$), and ice adhesion strength. Furthermore this correlation passed through the origin, suggesting that the water parameter ($1 + \cos\theta_{rec}$) is physically meaningful for ice adhesion. The importance of this result is that simple measurements of receding contact angles of water droplets on substrates become a powerful tool for the design of ice-phobic surfaces.

Here we follow the methodology of Meuler et al and measure tetrahydrofuran hydrate adhesion strength on surfaces with a range of wettabilities. We find that hydrate adhesion

strength decreases with surface energy and can be predicted using the practical work of adhesion of a suitable probe fluid. These studies provide valuable insights into the systematic design of hydrate-phobic surfaces.

2. Experimental

2.1. Adhesion testing methodology

Tetrahydrofuran (THF) hydrate is used as a model system because THF is completely miscible in water and forms hydrate at atmospheric pressure and temperatures below 4.4 ˚C for a solution of 19.1% THF (by weight) in water[25]. THF hydrate adhesion is tested using a custom-built adhesion testing apparatus housed in a glove box containing a nitrogen environment. A solution of 19.1 wt.% THF in DI water is poured into glass cuvettes and frozen to the test substrates using the protocol shown schematically in **Fig. 1** (modified from reference 23). The liquid columns were frozen for 2 hours at -15 ˚C to yield an array of hydrate columns encased in cuvettes and adhered to the test substrates. The substrate temperature was monitored using a thermocouple attached to the top of one of the substrates. To minimize frost formation on the test substrates and apparatus, the relative humidity was kept below 5%.

The force required to detach each hydrate column from its test substrate was measured by driving a 12 mm wide wedge-shaped probe head of a force transducer (Imada, model ZP–44) into contact with the side of the hydrate-filled cuvette at a constant velocity of 1 mm s^{-1} and continuing to drive the probe forward until the hydrate breaks free from substrate. Hydrate adhesion strength was obtained by dividing the measured maximum force with the cross-sectional area (1 cm^2) of the hydrate-substrate interface established by the cuvette size. Fracture was observed to be predominantly adhesive, that is, no hydrate film remained on the surfaces after adhesion testing.

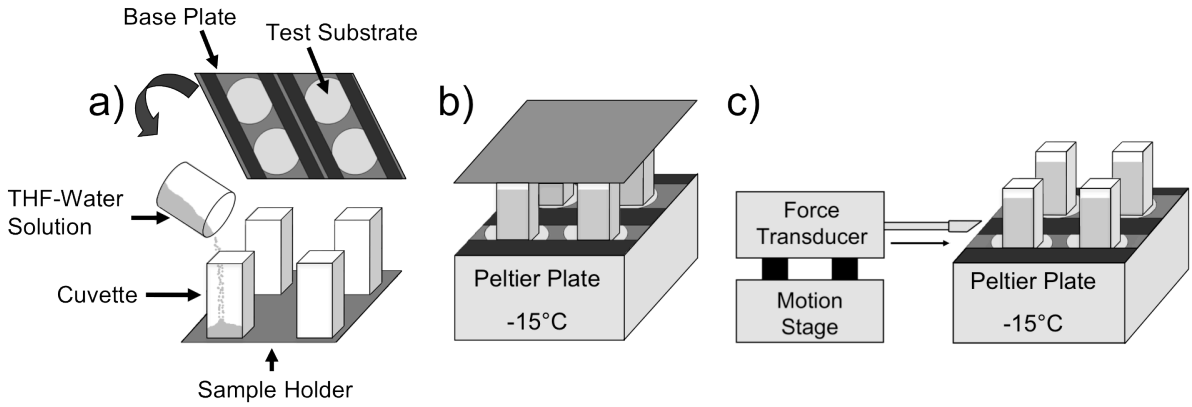

Figure 1. Schematic depiction of the procedure used to freeze hydrate columns on test substrates and to measure the hydrate adhesion strength (adapted from reference 23). The actual apparatus can hold a 4 x 5 array of samples; a 2 x 2 array is used here for ease of illustration. (a) A 19.1 wt.% solution of THF in DI water is poured into cuvettes housed in a sample holder (bottom) and the test substrates are clamped onto a base plate (top). The samples attached to the base plate are then mounted flush against the tops of the cuvettes. (b) The base plate-sample holder assembly is taken into a glove box operating under a nitrogen atmosphere, inverted, and bolted to a Peltier cooling plate whose surface is thermostated at -15 °C. The top sample holder is then removed, an insulating foam box is placed over the assembly to reduce the cooling load required of the chiller, and the hydrate columns are allowed to freeze for two hours. (c) The insulating box is removed and the wedge-shaped probe of a force transducer is propelled at 1 mm s^{-1} into the side of each cuvette at a height of 9.3 mm until the hydrate detaches from the test surface. The maximum force is recorded and converted into hydrate adhesion strength using the known cross-sectional area of the hydrate-substrate interface.

A photograph of the test apparatus is provided in **Fig. 2**(a). Side view photographs of the base of the cuvettes were taken as the THF-water solution was subcooled during the hydrate freezing process to demonstrate the mechanism of hydrate formation (Fig. 2(b) through Fig. 2(f)). The hydrate forms on the surface (Fig. 2(c)), which is at the lowest temperature, and grows into the solution (Fig. 2(d) through 2(e)), confirming that heterogeneous nucleation occurred on the surface. The hydrate continues to grow until the columns of solution are completely solidified (Fig. 2(f)).

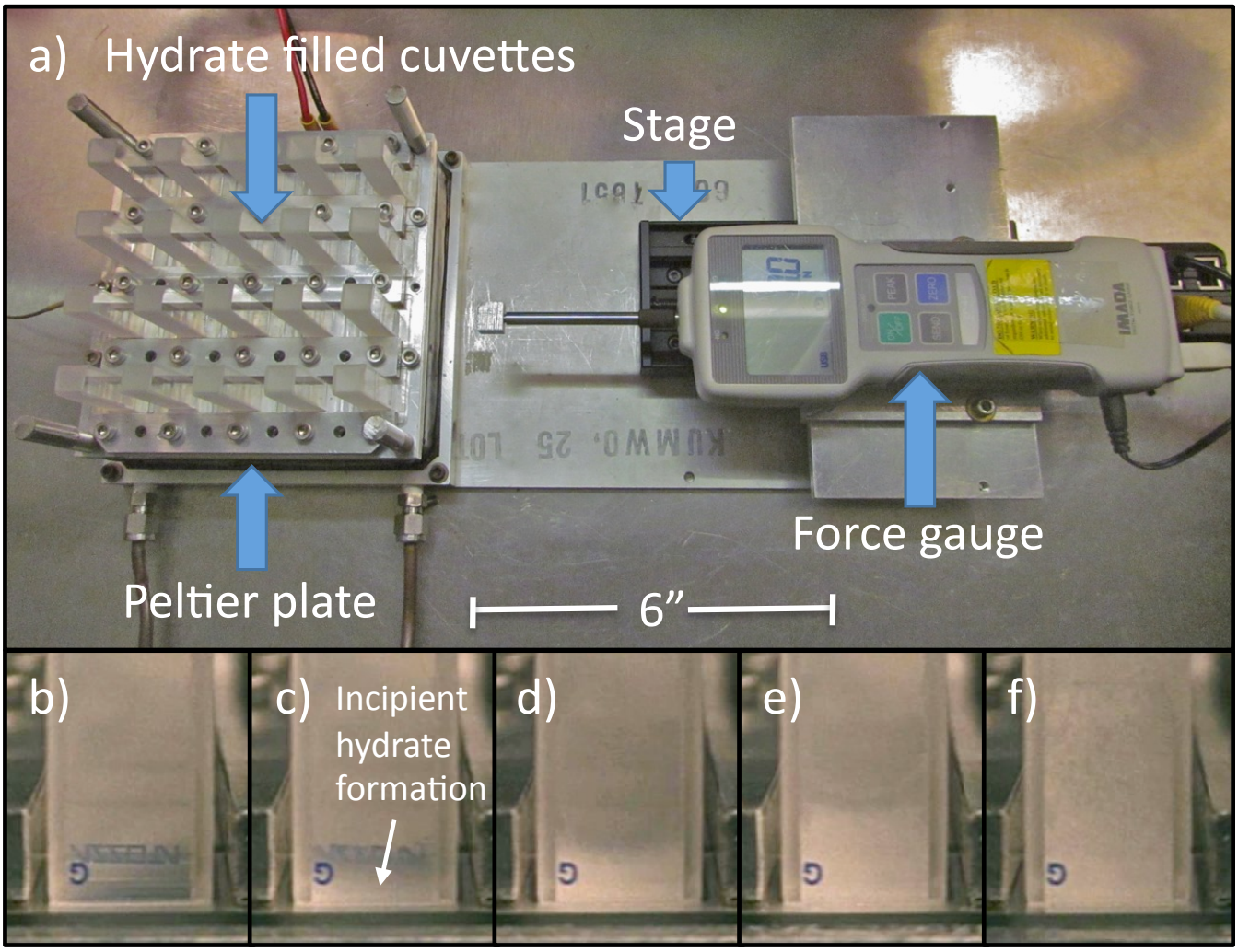

Figure 2. a) Photograph of the test apparatus and (b-f) side view photographs of the base of the cuvettes taken during the hydrate freezing process on a trichloro (1H, 1H, 2H, 2H-perfluoroctyl) silane-treated substrate b) sub-cooled THF-water solution before the onset of hydrate formation c) The THF hydrate begins to grow from the substrate surface, confirming that heterogeneous nucleation occurred at the solution-substrate interface d-f) hydrate growth continues until the columns of solution are completely solidified.

2.2. Substrate selection and preparation

A library of test surfaces with varying chemistry was established in order to elucidate the influence of surface properties, such as wettability and surface energy, on adhesion strength. These surfaces, ranging from hydrophilic to hydrophobic, include thiolated gold, silane-treated glass, and a blend of 80%/20% poly (ethyl methacrylate) (PEMA)/fluorodecyl polyhedral oligomericsilsesquioxane (fluorodecyl POSS) [26] spin coated onto steel. The substrate fabrication, cleaning, and storage protocols are provided in the supplemental materials. Surface energies of each of the test substrates were calculated using van Oss–

Chaudhury–Good (vOCG) analysis [27] from measured advancing and receding contact angles of up to 5 test fluids (described in the following section), Advancing and receding contact angles of DI water and surface energies calculated from advancing and receding contact angles of the test fluids are provided in **Fig. 3** for each of the surfaces tested.

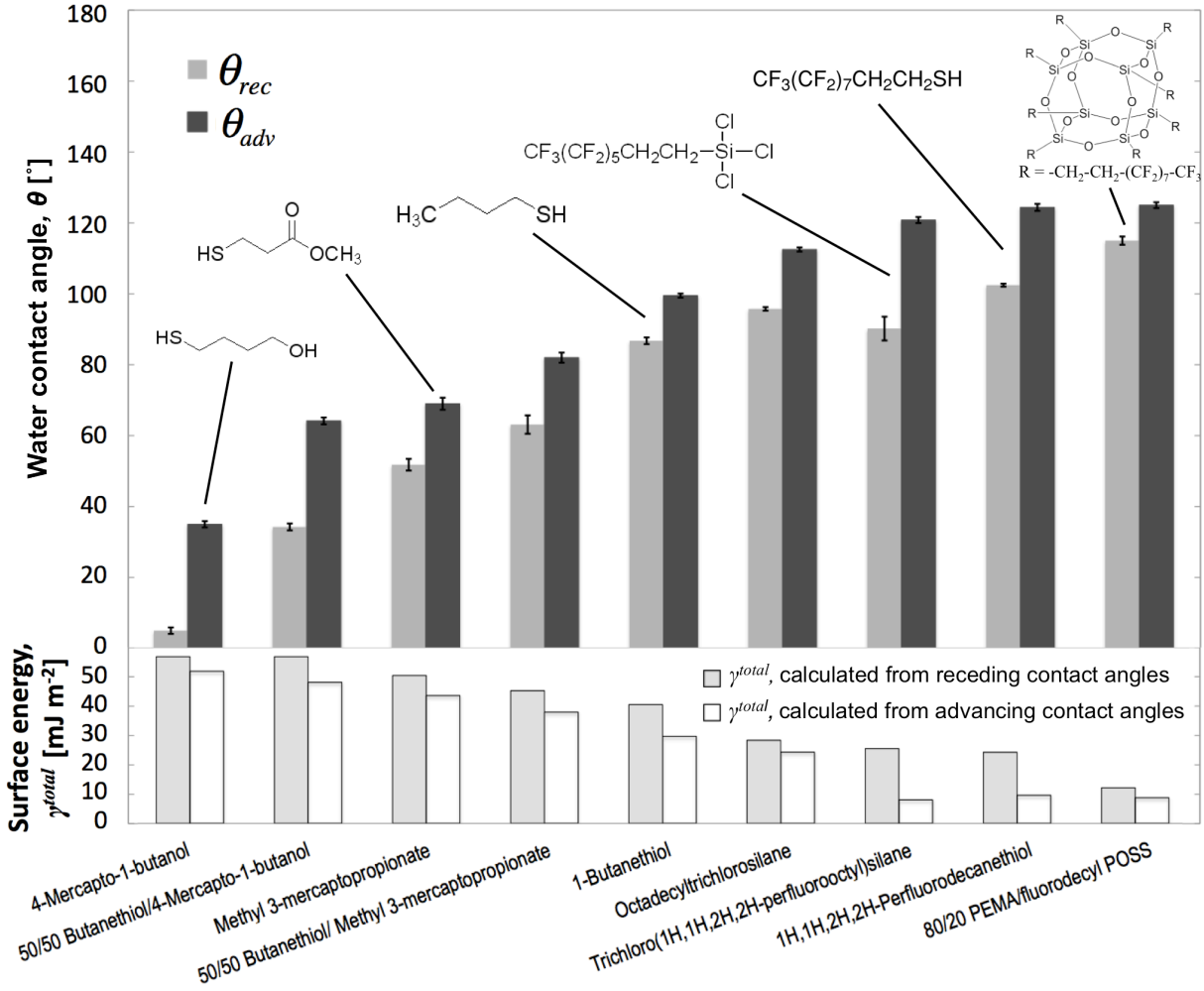

Figure 3. Advancing and receding contact angle measurements of DI water on each of the test substrates (top). Surface energies of each of the of the test substrates calculated using vOCG analysis of measured advancing and receding contact angles of polar and nonpolar test fluids (bottom). Advancing contact angles range from 35˚ to 125˚ and receding contact angles range from 5˚ to 115˚. Advancing surface energies range from 8 mJ m^{-2} to 50 mJ m^{-2}. Receding contact angles of several of the test fluids on 4-Mercapto-1-butanol were zero, thus its receding surface energy could not be determined precisely, and the plotted value represents its minimum receding surface energy.

2.3. Contact angle measurements

Contact angles of four polar fluids: DI water (18 MΩ-cm, Millipore), ethylene glycol (Alfa Aesar), formamide (Alfa Aesar), and a 19.1 wt.% mixture of THF (Alfa Aesar) in DI water, and two nonpolar fluids: 1-bromonaphthalene (Alfa Aesar) and diiodomethane (Alfa Aesar), were measured on the test surfaces using a Ramé-Hart Model 500 Advanced Goniometer/Tensiometer. Advancing (θ_{adv}) and receding (θ_{rec}) angles were taken as an average of at least 8 measurements. 5 μl droplets were deposited at a volume addition/subtraction rate of 0.2 μl s^{-1}, yielding contact line velocities less than 1 mm min^{-1}. The resulting capillary numbers ($Ca = \mu V/\gamma$) were less than 10^{-5} for all fluids tested, ensuring that the measured dynamic contact angles were essentially the same as contact angles obtained immediately after the contact line comes to a stop [28-31]. Advancing and receding surface energies were computed using vOCG analysis [27] of the gathered advancing and receding contact angle data. The Lifshitz-van der Waals, Lewis acid, and Lewis base contributions, as well as the total solid phase surface energy (γ^{LW}, $\sqrt{\gamma^+}$, $\sqrt{\gamma^-}$, and γ^{total} respectively) are provided in Table 1. Different values are obtained depending on whether advancing or receding values of test fluids are used in the vOCG analysis. Some receding surface energies could not be determined because non-zero receding contact angles of at least one nonpolar and two polar probe fluids were not always attained.

The surface tension, and therefore the contact angle, of the THF-water solution varies with time due to evaporation of THF from the solution. The variation of surface tension with time was measured using the pendant drop method [32] (Fig. S1). Based on these measurements, care was taken to measure advancing and receding contact angles of the THF-water solution before significant evaporation of THF from the solution could occur (see supplementary materials for details).

Table 1. Surface energy properties of the tested substrates, calculated from advancing and receding contact angles of DI water, ethylene glycol, formamide, 1-bromonaphthalene, and diiodomethane using vOCG analysis, where $\gamma^{total} = \gamma^{LW} + 2\sqrt{\gamma^{+}}\sqrt{\gamma^{-}}$. Receding surface energies of steel, glass, and 4-mercapto-1-butanol could not be determined because non-zero receding contact angles of at least one nonpolar and two polar test fluids were not attained on these surfaces. The error in these surface energy data is on the order of 15%.

Substrate	Advancing surface energy data				Receding surface energy data			
	γ^{LW} [mJ m^{-2}]	$\sqrt{\gamma^{+}}$ [mJ$^{1/2}$ m^{-1}]	$\sqrt{\gamma^{-}}$ [mJ$^{1/2}$ m^{-1}]	γ^{total} [mJ m^{-2}]	γ^{LW} [mJ m^{-2}]	$\sqrt{\gamma^{+}}$ [mJ$^{1/2}$ m^{-1}]	$\sqrt{\gamma^{-}}$ [mJ$^{1/2}$ m^{-1}]	γ^{total} [mJ m^{-2}]
1-Butanethiol	32	-0.6	1.5	30	42	-0.3	1.9	41
1*H*,1*H*,2*H*,2*H*-Perfluorodecanethiol	10	0.5	0.0	10	25	-0.3	1.4	24
Methyl 3-mercaptopropionate	44	0.0	3.7	44	44	0.6	4.9	50
4-Mercapto-1-butanol	46	0.4	6.4	52	N/A	N/A	N/A	N/A
50/50 Butanethiol/Methyl 3-mercaptopropionate	40	-0.4	2.8	38	47	-0.2	4.3	45
50/50 Butanethiol/4-Mercapto-1-butanol	44	0.5	3.7	48	51	0.5	6.1	57
Trichloro (1*H*,1*H*,2*H*,2*H*-perfluorooctyl) silane	8	0.8	0.3	8	25	0.1	2.4	26
Octadecyltrichlorosilane	24	-0.3	0.2	24	30	-0.4	1.9	28
80/20 PEMA/fluorodecyl POSS	9	0.1	0.3	9	13	-0.2	1.1	12
Clean glass	41	0.7	7.8	51	N/A	N/A	N/A	N/A
Bare steel	39	-0.3	3.9	37	N/A	N/A	N/A	N/A

Surface roughness characterization

Surface texture plays an important role in adhesion and can often result in interlocking of the adhering materials, increasing adhesion strength. This was demonstrated recently in our studies of ice adhesion [33], in which we observed an linear increase in adhesion strength with the Wenzel roughness, that is, the total surface area divided by the occluded area [34]. For the purpose of this study, we are interested in studying the effects of surface chemistry alone, and therefore focus on smooth surfaces. Surface profilometry was conducted to verify the smoothness of our test surfaces. A Tencor P-12 profilometer with a 2 μm radius stylus and a Zygo interferometer were used to measure the roughness of the steel discs and the 80%/20%

PEMA/fluorodecyl POSS coated steel discs. Atomic force microscopy (AFM) was carried out on glass, gold, and some representative silanes and thiols using a VeecoDimension 3100 scanning probe microscope operating in the tapping mode. The Wenzel roughness is $r < 1.06$ for all surfaces tested. The measured roughness data are presented in **Table S2** of the supplementary materials.

3. Results and discussion

Results of the adhesion tests for all test surfaces are provided in **Table S3** of the supplementary materials along with measured advancing and receding contact angles of water and 19.1 wt.% THF in water solution, and calculated advancing and receding surface energy data. Adhesion strength ranged from 422 ± 69 kPa on steel, which has a measured advancing surface energy of 36 mJ m^{-2}, to 90 ± 16 kPa on steel coated with an 80/20 PEMA/fluorodecyl POSS blend, which has a measured advancing surface energy of 9 mJ m^{-2}. This four-fold reduction in adhesion strength demonstrates the importance of surface chemistry to adhesion. However, to *design* surfaces for reduced adhesion, the key surface properties that affect adhesion must be determined.

The theory of brittle cohesive fracture published by Griffith in 1920 proposed that the cohesive strength of a brittle material, that is, the critical stress required to initiate cohesive fracture, is a function of the work of cohesion.[35] Griffith's fracture criterion was later extended to adhesive fracture with plastic deformation of the adhering materials, showing that adhesion strength is a function of the work of adhesion.[36-38] Accordingly, there is expected to be a correlation between the work of adhesion between two materials and their adhesion strength.

The work of adhesion between two smooth bodies is known to depend strongly on van der Waals (apolar), electron acceptor (Lewis acid), and electron donor (Lewis base) interactions[39]. The latter interactions are generally alluded to as *polar* interactions and arise

primarily due to hydrogen bonding [40], and are therefore especially important when considering polar materials such as water, ice, or hydrates. The sum of these interactions can be characterized by the thermodynamic work of adhesion, W^a, which is a function of the Lifshitz van der Waals, Lewis acid, and Lewis base parameters of surface energy of the adhering materials, denoted by γ^{LW}, γ^+, and γ^- respectively. The work of adhesion of a material A to a material B is given by[27]

$$W_{AB}^a = 2\left(\sqrt{\gamma_A^{LW}\gamma_B^{LW}} + \sqrt{\gamma_A^+\gamma_B^-} + \sqrt{\gamma_A^-\gamma_B^+}\right) \quad (1)$$

where the subscripts A and B denote the two adhering materials.

Note that the work of adhesion of material A to itself is simply the work of cohesion of material A, W_A^c. Then by reducing the right side of Eq. 1, with both subscripts denoting material A, we obtain,

$$W_A^c = 2\left(\gamma_A^{LW} + 2\sqrt{\gamma_A^+\gamma_A^-}\right) \equiv 2\gamma_A^{total} \quad (2)$$

where γ_A^{total} is the total surface energy of material A in equilibrium with its vapor. If one of the materials (A) in Eq. 1 is a liquid that exhibits a non-zero contact angle, θ_{AB}, then the work of adhesion is also given by the Young-Dupré equation:[40]

$$W_{AB}^a = \gamma_A^{total}(1+\cos\theta_{AB}) \quad (3)$$

If $\theta_{AB} = 0$ then A may spread on B and $W_{AB}^a > W_{AA}^c$.[41] Therefore, if $\theta_{AB} = 0$, then $W_{AB}^a \geq \gamma_A^{total}(1+\cos\theta_{AB}) = 2\gamma_A^{total} = W_{AA}^c$. Thus Eq. 3 cannot be used to calculate the work of adhesion when complete wetting occurs, that is, when $\theta_{AB} = 0$.

The surface energy parameters of the THF hydrate (as in Eq. 1) cannot be determined readily due to the evaporation of THF from the frozen hydrate surfaces prior to contact angle measurements of the test fluids used in the vOCG analysis. Further difficulties arise in selecting test fluids that remain liquid at temperatures below the melting temperature of THF hydrate, 4.4 ˚C, that are insoluble in THF. Hence, having a probe liquid that can mimic the

adhesion properties of the THF hydrate is desirable for predicting the hydrate-phobicity (i.e., the ability to reduce hydrate adhesion) of a surface. For example, in studies of ice adhesion, liquid water is used as a probe fluid. Specifically, correlations are made between the adhesion strength of *ice* on a selected substrate and the work of adhesion of *liquid water* on that same substrate, though a fundamental basis for this approach has not been established.

In order to apply a similar approach to predicting hydrate adhesion, we digress here and study ice and water as a model system to provide support for a probe fluid approach and to gain insights into the selection of an appropriate probe fluid for hydrates. As discussed previously, the adhesion strength of a material to a substrate is a function of its thermodynamic work of adhesion to that substrate. However, for studies of ice adhesion, the work of adhesion of *liquid water* on a selected substrate is correlated with the adhesion strength of *ice* on that same substrate. Here we hypothesize that the existence of this correlation is attributable to the similarity of the surface energy parameters of ice and liquid water. For water at 25°C, $\sqrt{\gamma^{LW}}$ = 4.67 $mJ^{1/2}$ m^{-1}, $\sqrt{\gamma^{+}}$ = 5.05 $mJ^{1/2}$ m^{-1}, $\sqrt{\gamma^{-}}$ = 5.05 $mJ^{1/2}$ m^{-1}, and γ^{total} = 72.8 mJ m^{-2}, and for ice at 0 °C, $\sqrt{\gamma^{LW}}$ = 5.44 $mJ^{1/2}$ m^{-1}, $\sqrt{\gamma^{+}}$ = 3.74 $mJ^{1/2}$ m^{-1}, $\sqrt{\gamma^{-}}$ = 5.29 $mJ^{1/2}$ m^{-1}, and γ^{total} = 69.2 mJ m^{-2}.[42] Consequently, the work of adhesion of liquid water to most materials is approximately equal to that of ice according to Eq. 1. This near-equality is demonstrated by calculating the work of adhesion of liquid water and that of ice to the surfaces tested in this work. Using Eq. 1, the work of adhesion of ice is calculated using the surface energy parameters of ice listed above and the surface energy parameters calculated for each of the substrates using vOCG analysis (Table 1). The resulting values are plotted against the work of adhesion for water, determined from its advancing and receding contact angles on the test substrates (**Fig. 4**). The strong linear correlation (R^2 = 0.98) suggests that work of adhesion measurements for liquid water are a good approximation of the work of adhesion of ice. According to fracture mechanics theory, adhesion strength of ice

is a function of the work of adhesion of ice.[36-38] Consistent with this theory and the near-equality between the works of adhesion of water and ice, the adhesion strength of ice should therefore correlate with the work of adhesion of liquid water. That is, $\tau_{ice} = f(W_{ice}^{a}) \cong g(W_{water}^{a})$, where τ_{ice} is the strength of ice adhesion, W_{ice}^{a} is the work of adhesion of ice, and W_{water}^{a} is the work of adhesion of liquid water. Different values for work of adhesion can be determined depending on the contact angle (advancing, receding, static), used in Eq. 3. Meuler et al[23] have concluded that ice adhesion strength correlates most strongly with the work of adhesion calculated from receding contact angle measurements, $\gamma_{water}(1 + \cos\theta_{rec})$, that is, with the practical work of adhesion[43] for liquid water.

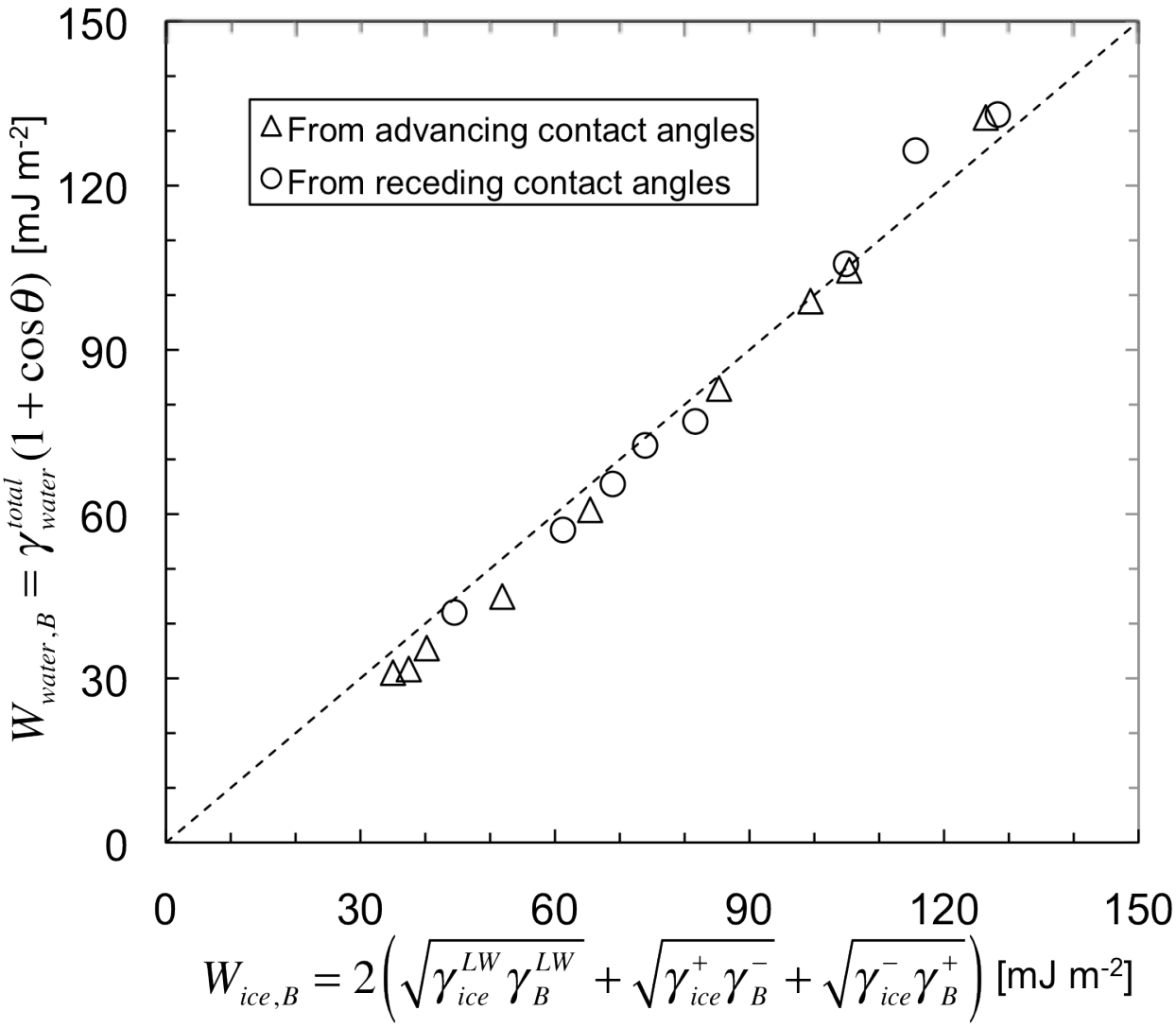

Figure 4. Work of adhesion of liquid water, $W_{water,B}$, plotted against the work of adhesion of ice to each test substrate, $W_{ice,B}$, where B represents the test substrates. The work of adhesion of liquid water was calculated using vOCG analysis measured advancing and receding water contact angles on each test substrate. The work of adhesion of ice was calculated using the surface energy properties of ice and the advancing and receding surface energy properties of each test substrate. The similarities between the work of adhesion of liquid water and ice explain why water is an effective probe fluid for gauging ice adhesion.

Motivated by these ice adhesion studies, a probe fluid was selected to be used in approximating the work of adhesion of solid hydrate to various substrates. The 19.1 wt.% THF in water solution used to form THF hydrate was the natural choice. In **Fig. 5**, THF hydrate adhesion strength is plotted against the normalized practical work of adhesion, $1 + \cos\theta_{rec}$, of the 19.1 wt.% THF in water solution. A linear fit through the origin shows an excellent correlation ($R^2 = 0.90$) consistent with the fact that hydrate adhesion strength must approach zero as the work of adhesion of a probe fluid approaches zero (supplementary materials). In comparison, if DI water is used as a probe fluid (**Fig. 6**) a linear correlation passing through the origin is relatively poor ($R^2 = 0.51$). The surface energy properties of the 19.1 wt.% THF in water solution were estimated using a "reverse vOCG analysis" of its advancing and receding contact angles on each of the test surfaces (see supplementary material). The resulting surface energy parameters are $\sqrt{\gamma^{LW}} = 4.3$ mJ$^{1/2}$ m^{-1}, $\sqrt{\gamma^{+}} = 1.6$ mJ$^{1/2}$ m^{-1}, $\sqrt{\gamma^{-}} = 9.1$ mJ$^{1/2}$ m^{-1}, and $\gamma^{total} = 47$ mJ m^{-2}. The polar terms are significantly different from the aforementioned polar surface energy parameters of water, resulting in different work of adhesion measurements on the test surfaces. The correlation in Fig. 5 exists because the polar and van der Waals surface energy properties of the 19.1 wt.% THF in water solution reflect those of THF hydrate, just as liquid water reflects the surface energy properties of ice. Thus, the practical work of adhesion of 19.1 wt.% THF in water solution can be used to estimate the adhesion strength of THF hydrate. The lowest hydrate adhesion strength was observed on the 80%/20% PEMA/fluorodecyl POSS treated steel disc, which exhibited the highest receding contact angle of the THF-water solution (90˚). The positive

slope and monotonic behavior of the data plotted in Fig. 5 suggest that lower hydrate adhesion could be achieved on surfaces with lower practical work of adhesion to the THF-water probe fluid. This can be accomplished by minimizing the polar and nonpolar surface energy parameters of the coating.

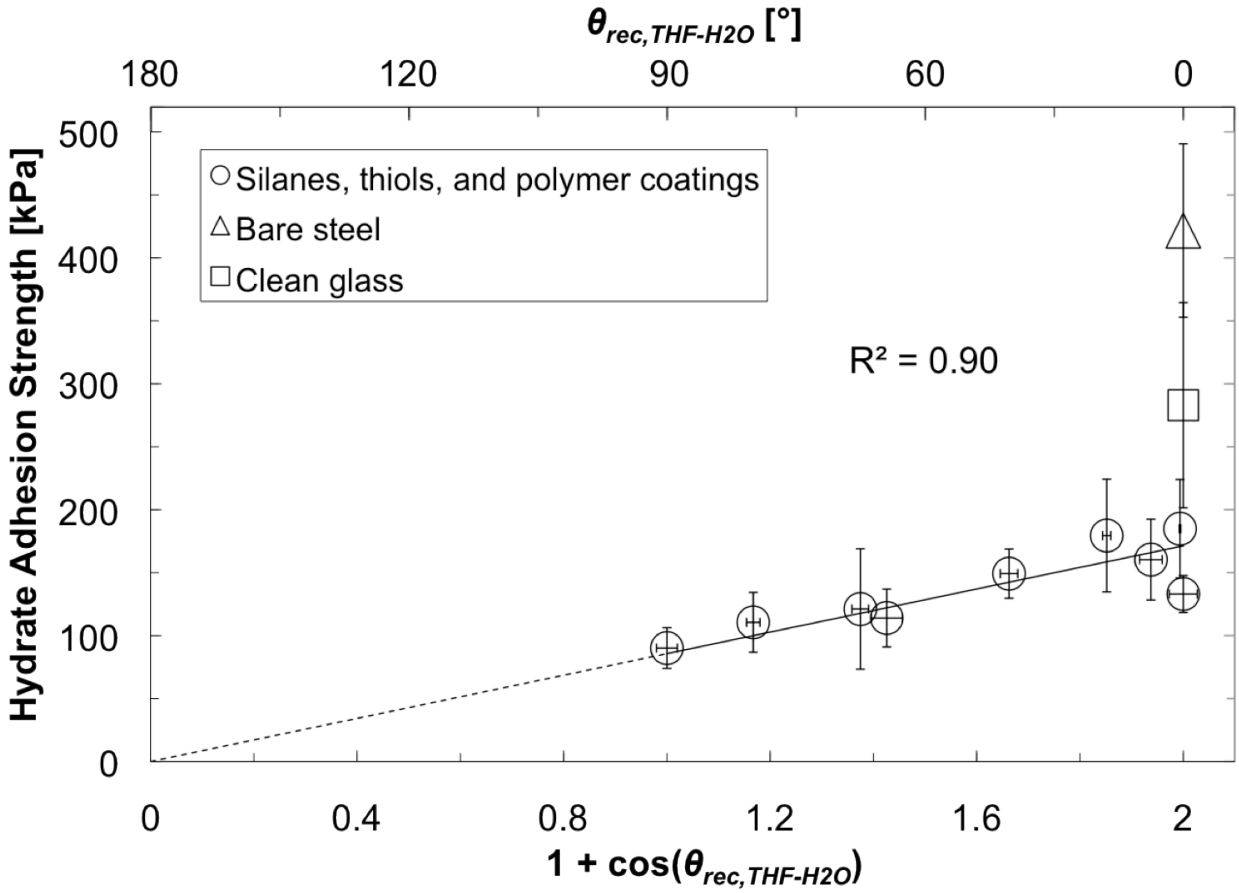

Figure 5. Hydrate adhesion strength plotted against the practical work of adhesion the 19.1 wt.% THF in water solution. The high surface energies of clean glass and steel result in their complete wetting by the THF-water solution ($\theta_{rec} = 0$). For these surfaces the normalized practical work of adhesion may be greater than two (1 + cos(0)). For this reason, these points were excluded from the correlation, while presented on the plot to demonstrate their much greater adhesion to hydrates compared to the treated substrates. More than four-fold reduction in adhesion strength was measured on low-surface energy coatings compared to bare steel. A linear fit through the origin shows an excellent correlation ($R^2 = 0.90$) consistent with the fact that hydrate adhesion strength must approach zero as the work of adhesion of a probe fluid approaches zero.

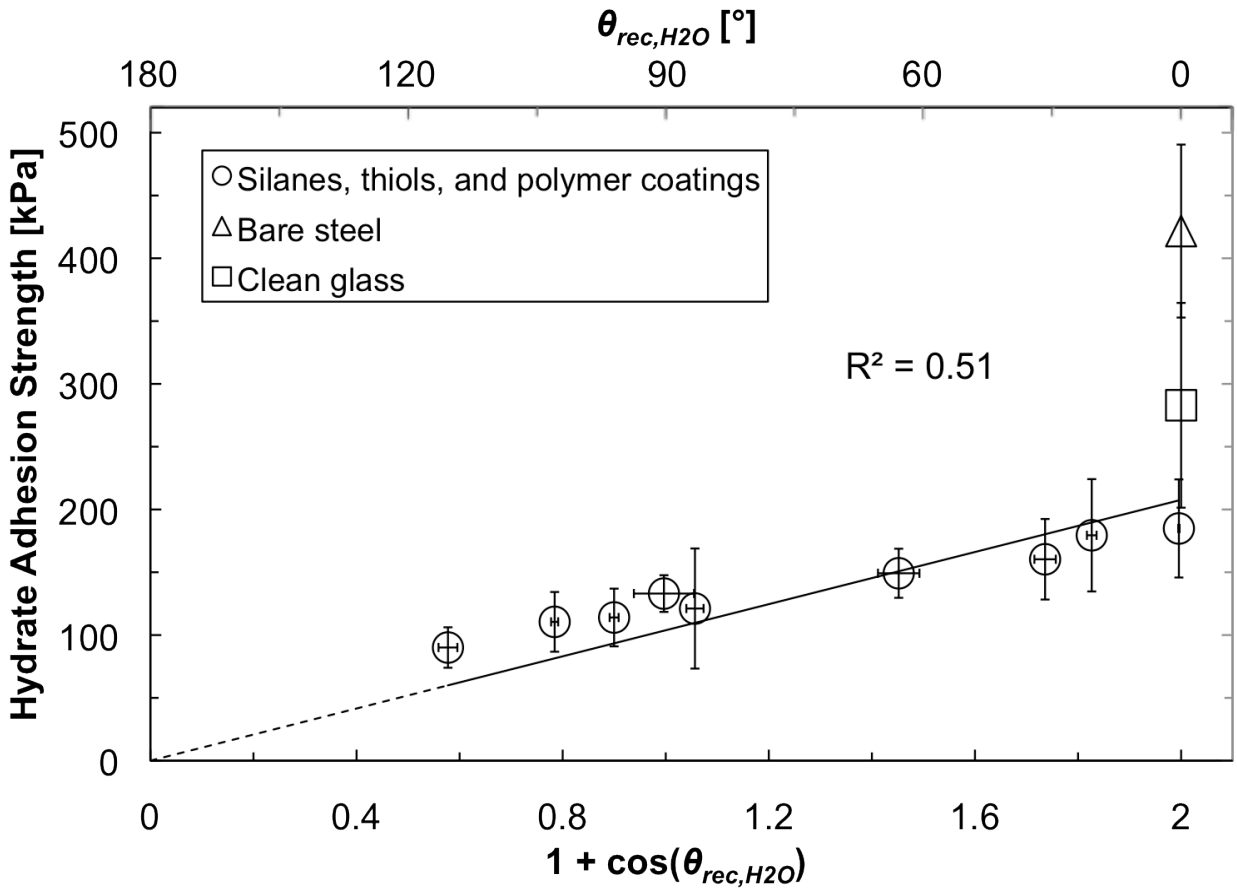

Figure 6. Hydrate adhesion strength plotted against the practical work of adhesion of liquid water. A linear fit to the data consistent with zero adhesion strength at zero work of adhesion is relatively poor, with a correlation coefficient of $R^2 = 0.51$.

Conclusions

We have demonstrated a reduction in adhesion strength of the THF hydrate by more than a factor of four on treated surfaces compared with bare steel. This reduction is achievable on surfaces characterized by low Lewis acid, Lewis base, and van der Waals interactions, such that the work of adhesion (Eq. 1) is minimized. The work of adhesion between two solid materials cannot be easily measured in practice, and is therefore not a practical tool for predicting adhesion strength. However, hydrate adhesion strength was correlated with the normalized practical work of adhesion of a suitable probe fluid with similar surface energy properties to those of the hydrate, which can therefore serve as simple and valuable tool for

predicting hydrate adhesion strength and rapidly screening surface treatments or coatings for hydrate-phobicity.

Unlike THF hydrate, a liquid with identical chemistry to a gas hydrate is unstable, as the solubility of a hydrate-stabilizing gas in liquid water is much lower than its concentration in the hydrate phase. Thus, the surface energies of gas hydrates, such as methane hydrate, must be measured using vOCG analysis, and a liquid solution designed with commensurate surface energy properties (characterized using a "reverse vOCG" analysis). This solution can then serve as a probe fluid to predict the adhesion strengths of gas hydrates to various materials, providing a much simpler alternative to high pressure gas hydrate adhesion testing. This approach can therefore lead to rapid screening of potential hydrate-phobic surfaces, such as those with specific chemistry chosen to minimize polar and van der Waals interactions governing the work of adhesion.

The expected trend beyond the range of the data acquired (extrapolated with a dashed line in Fig. 5) suggests that further reductions in hydrate adhesion could be achieved by minimizing polar and nonpolar parameters of surface energy. Hydrate adhesion may be further reduced by tailoring nano- and microscale surface morphology and chemistry to prevent penetration of the hydrate into the texture (as we have seen with ice [33]) such that the hydrate rests atop the texture features to reduce contact at the hydrate-substrate interface. This approach has already been successful for reducing ice adhesion on superhydrophobic surfaces [45-50] under conditions unfavorable to frost formation. Other approaches such as designing hybrid low/high surface energy morphologies that can spatially control nucleation [44, 45] (e.g. promote nucleation atop surface features) could be used to reduce hydrate adhesion under conditions favorable to desublimation or condensation.

The results of this work suggest possible extension of the probe fluid approach to predicting adhesion strength between many other materials: the practical work of adhesion of a material in its liquid state to a substrate could be used to estimate the adhesion strength of the same

material in its solid state to a substrate. The approach to predicting adhesion strength and methods of controlling adhesion strength laid out in this paper could benefit many industrial applications such as de-icing, welding, composite materials, thin films and coatings, and salt scaling.

As the world's energy demands are rapidly increasing, there is a strong shift towards the expansion of deep-sea drilling. Cheaper and more effective methods of gas hydrate mitigation must be found in order for this movement to be economical and safe. The principles discussed in this paper provide a framework for the development of hydrate-phobic surfaces, which in turn provides a pathway to passive enhancement of flow assurance and prevention of catastrophic failures in deep-sea oil and gas operations.

Acknowledgements

The authors gratefully acknowledge financial support from the MIT Energy Initiative-Chevron program. KKV acknowledges support from MIT Mechanical Engineering startup funds towards building the adhesion test apparatus. We thank Dr. Joe Mabry of Edward Airforce Base for providing fluorodecyl POSS and we acknowledge fruitful discussions with Prof. Ali S. Argon at MIT about adhesion and fracture mechanics, Dr. Shreerang S. Chhatre of MIT about wetting and vOCG surface energy analysis, and Dr. Owen Oakley of Chevron about applications to the oil and gas industry.

[1] World Energy Outlook Homepage. Available from: http://www.worldenergyoutlook.com/.
[2] E. D. Sloan, C. A. Koh, *Clathrate hydrates of natural gases*, CRC Press, Boca Raton, FL 2008.
[3] E. D. Sloan, Nature 2003, 426, 353.
[4] H. Weber, S. Larimer. BP working to formulate new approach to spill. 2010; Available from: http://www.msnbc.msn.com/id/37049432/ns/disaster_in_the_gulf/t/bp-working-formulate-new-approach-spill/.
[5] A. K. Sum, C. A. Koh, E. D. Sloan, Industrial & Engineering Chemistry Research 2009, 48, 7457.
[6] B. C. Gbaruko, J. C. Igwe, P. N. Gbaruko, R. C. Nwokeoma, Journal of Petroleum Science and Engineering 2007, 56, 192.
[7] C. A. Koh, R. E. Westacott, W. Zhang, K. Hirachand, J. L. Creek, A. K. Soper, Fluid Phase Equilibria 2002, 194-197, 143.

[8] V. M. Bilyushov, Journal of Engineering Physics and Thermophysics 1984.
[9] P. Bishnoi, V. Natarajan, Fluid Phase Equilibria 1996, 117, 168.
[10] D. Kashchiev, A. Firoozabadi, Journal of Crystal Growth 2002, 241, 220.
[11] D. Kashchiev, A. Firoozabadi, Journal of Crystal Growth 2002, 243, 476.
[12] M. Anklam, A. Firoozabadi, The Journal of Chemical Physics 2004, 121, 11867.
[13] B. J. Anderson, J. W. Tester, G. P. Borghi, B. L. Trout, J. Am. Chem. Soc 2005, 127, 17852.
[14] S. R. Davies, K. C. Hester, J. W. Lachance, C. A. Koh ,Ä¶, Chemical Engineering Science 2009.
[15] M. Walsh, C. Koh, E. Sloan, A. Sum, D. Wu, Science 2009, 326, 1095.
[16] T. Koga, J. Wong, M. K. Endoh, D. Mahajan, C. Gutt, S. K. Satija, Langmuir 2010, 26, 4627.
[17] S.-o. Yang, D. M. Kleehammer, Z. Huo, E. D. Sloan, K. T. Miller, Journal of Colloid and Interface Science 2004, 277, 335.
[18] C. Taylor, L. Dieker, K. Miller, C. Koh, E. Sloan, Journal of Colloid and Interface Science 2007, 306, 255.
[19] C. J. Taylor, L. E. Dieker, K. T. Miller, C. A. Koh, E. D. Sloan, "Hydrate Particles Adhesion Force Measurements: Effects Of Temperature, Low Dosage Inhibitors, and Interfacial Energy", 2008.
[20] L. E. Dieker, Z. M. Aman, N. C. George, A. K. Sum, E. D. Sloan, C. A. Koh, Energy & Fuels 2009, 23, 5966.
[21] J. W. Nicholas, L. E. Dieker, E. D. Sloan, C. A. Koh, Journal of Colloid and Interface Science 2009, 331, 322.
[22] G. Aspenes, L. E. Dieker, Z. M. Aman, S. H≈ôiland, A. K. Sum, C. A. Koh, E. D. Sloan, Journal of Colloid and Interface Science 2009.
[23] A. J. Meuler, J. D. Smith, K. K. Varanasi, J. M. Mabry, G. H. McKinley, R. E. Cohen, ACS Applied Materials & Interfaces 2010, 2, 3100.
[24] V. F. Petrenko, R. W. Whitworth, *Physics of ice*, 1999.
[25] E. D. Sloan, C. A. Koh, *Clathrate hydrates of natural gases*, 2008.
[26] J. Ä. Mabry, A. Vij, S. Ä. Iacono, B. Ä. Viers, Angewandte Chemie 2008, 120, 4205.
[27] R. J. Good, Journal of Adhesion Science and Technology 1992, 6, 1269.
[28] M. Strobel, C. S. Lyons, Plasma Processes and Polymers 2011, 8, 8.
[29] F. Garbassi, M. Morra, E. Occhiello, *Polymer surfaces from physics to technology*, Wiley, 1994.
[30] Y. Uyama, H. Inoue, K. Ito, A. Kishida, Y. Ikada, Journal of Colloid and Interface Science 1991, 141, 275.
[31] L. M. Lander, L. M. Siewierski, W. J. Brittain, E. A. Vogler, Langmuir 1993, 9, 2237.
[32] C. E. Stauffer, The Journal of Physical Chemistry 1965, 69, 1933.
[33] K. K. Varanasi, T. Deng, J. D. Smith, M. Hsu, N. Bhate, Applied Physics Letters 2010, 97, 234102.
[34] R. N. Wenzel, Industrial & Engineering Chemistry 1936, 28, 988.
[35] A. A. Griffith, Philosophical Transactions of the Royal Society of London. Series A, Containing Papers of a Mathematical or Physical Character 1921, 221, 163.
[36] S. J. Bennett, K. L. Devries, M. L. Williams, International Journal of Fracture 1974, 10, 33.
[37] D. Maugis, M. Barquins, Journal of Physics D: Applied Physics 1978, 11, 1989.
[38] A. A. Volinsky, N. R. Moody, W. W. Gerberich, Acta Materialia 2002, 50, 441.
[39] K. L. Mittal, *Acid-base Interactions: Relevance to Adhesion Science and Technology*, Vol. 2, 2000.
[40] D. H. Bangham, R. I. Razouk, Transactions of the Faraday Society 1937, 33, 1459.

[41] E. D. Shchukin, *Colloid and surface chemistry*, 2001.
[42] C. J. Van Oss, R. F. Giese, R. Wentzek, J. Norris, E. M. Chuvilin, Journal of Adhesion Science and Technology 1992, 6, 503.
[43] K. L. Mittal, ASTM Special Technical Publication 1976, 640, 5.
[44] J. Aizenberg, A. J. Black, G. M. Whitesides, Nature 1999, 398, 495.
[45] K. K. Varanasi, M. Hsu, N. Bhate, W. S. Yang, T. Deng, Applied Physics Letters 2009, 95.